Hindawi
Journal of Sensors
Volume 2019, Article ID 7893462, 18 pages
https://doi.org/10.1155/2019/7893462

Research Article

Suppression Method of Jump Points for Multipole Magnetic Encoder at Low Temperature Based on Single-Pole Angle Value Fitting

L. Wang, Q. M. Ren, J. C. Han, and Y. D. Zhang

Harbin University of Science and Technology, Harbin 150080, China

Correspondence should be addressed to J. C. Han; hanjichao163@163.com

Received 24 May 2018; Revised 9 November 2018; Accepted 26 November 2018; Published 19 March 2019

Academic Editor: Stephen James

To eliminate the jump points of multipole angle values after subdivision at low temperature, the magnetic field and temperature field characteristics of a multipole magnetic encoder are analyzed in this study, and the effect of changes in magnetic field strength and temperature field on the precision of angle values is studied. To eliminate the jump point of multipole angle values caused by changes in the temperature field, the suppression method based on single-pole angle value fitting is proposed. The error between the single-pole and multipole angle values is tabulated by the oversampling linear interpolation method, and the precision of fitting single-pole to multipole angle values is effectively improved. The error of the angle value caused by changes in the temperature field is studied and analyzed, and the relationship between the jump angle values and the pole number of the multipole magnetic encoder is obtained. Furthermore, the jump point is compensated for by the jump range of the multipole angle values. Finally, the angle accuracy of the multipole magnetic encoder in a cryogenic chamber is experimentally verified. The experimental results show that the low-temperature jump point compensation method proposed for the multipole magnetic encoder in this paper can effectively suppress the jump of the angle values.

1. Introduction

With the accelerated development of industrialization, people have high requirements for the resolution and precision of angular displacement sensor. At present, magnetic encoder and photoelectric encoder are widely used as angular displacement sensors [1]. The photoelectric encoder is of high precision, but the volume is large. The magnetic encoder can work in the dust and oil environment, but the resolution and precision of the magnetic encoder are difficult to be improved [2]. In order to improve the precision of the magnetic encoder, scholars have done a lot of research.

A rotary magnetic sensor with complementary metal oxide semiconductor is proposed; it can improve the precision of the sensor up to 10 bits/rotation through the offset calibration [3]. A high-accuracy magnetic rotary encoder is proposed. The structure with the magnetic collector can improve the magnetic field distribution. In order to eliminate the output deviation of the magnetic encoder, the signal correction algorithm based on the least square estimation is proposed [4]. An error compensation method for a single pair-pole encoder is proposed; it can compensate position error, and the precision of magnetic encoder which used this method could reach $\pm 1^{\circ}$ [5]. A magnetic encoder with a novel arrangement of Hall effect sensors is proposed. It is used to measure the angle value of rotation. The Hall effect sensors are equilaterally arranged; it can eliminate harmonics of the third order and its multiples and improves the accuracy of the magnetic encoder [6]. In order to eliminate the steady-state error caused by installation errors, an integrated Hall magnetic encoder error correction method is proposed [7]. A compensation method based on PMSM sensor less control is proposed. It can eliminate the angle deviation of the magnetic encoder. In order to eliminate the noise signals, the oversampling linear interpolation tabulation method is proposed. Finally, the precision of the magnetic encoder is

limited within 0.09 degrees [8]. A magnetic rotary encoder is proposed. It can be used at several thousand revolution per minute (RPM), and its precision is higher than the photoelectric encoder [9]. A magnetic rotary encoder is designed. In order to improve the stability of the original signal, a modified version of Kalman filter is proposed, and the response speed of the magnetic encoder is improved. Finally, the absolute error of the encoder is limited within 0.03 degrees [10]. A harmonic fitting algorithm is proposed which is used to estimate rotational angle; it can compensate for the eccentrically mounted angle of error [11]. An absolute magnetic rotary position sensor is designed. In order to measure absolute angular position, a method based on the vernier caliper measuring principle is proposed. A new error compensation model based on genetic algorithm is proposed; it can improve the precision of the magnetic encoder. Finally, the accuracy of the magnetic encoder can reach up to 0.2 degrees [12]. A real-time controller has been proposed to develop a correction and interpolation algorithm and successfully optimized the magnetic encoder signal. This algorithm can run at very low speed [13]. A new multisensor data fusion methodology based on fuzzy logic has been proposed; it can improve the precision of the magnetic encoder [14]. A novel algorithm based on polynomial approximations (PA) is proposed; this algorithm is used for an efficient error compensation of magnetic analog encoders. The proposed PA algorithm assisted with the phase-locked loop is capable of reducing the total position error to a range as small as $\pm 0.2^{\circ}$ [15]. A subdivision method based on software frequency doubling is proposed. It uses digital filtering to filter the disturbed sine and cosine signals and multiplied by trigonometric function multiplication, which effectively improves the resolution of the encoder [16]. The encoder noise is easily removed by distributing the six Hall elements evenly around the permanent magnets and calibrated with an optical encoder to realize a 13-bit precision magnetic encoder [17]. The wave equation of angular displacement with amplitude error, waveform distortion, and DC component is established, and the orthogonal error correction parameter is solved by the least square method, which improves the precision of the encoder [18]. The neuron iterative algorithm is used to compensate the error of the temperature drift of the Hall element [19]. A rotary magnetic sensor using MEMS technology is proposed [20], and its measure precision is $[-0.5^{\circ}, +0.5^{\circ}]$.

In order to eliminate the jump points of multipole angle values after subdivision at low temperature, the magnetic field and temperature field characteristics of multipole magnetic encoder are analyzed in this paper, and the effect of changes in magnetic field strength and temperature field on the precision of angle values is studied. In order to eliminate the jump point of multipole angle values caused by the change of temperature field, the suppression method based on single-pole angle value fitting has been proposed. The error between the single-pole angle values and the multipole angle values is tabulated by oversampling linear interpolation method, and the precision of fitting single-pole angle values to multipole angle values is effectively improved. The error of the angle value caused by the change of temperature field is studied and analyzed, and the relationship between the jump angle values and the pole number of the multipole magnetic encoder is obtained to compensate the jump point by the jump range of multipole angle values. The low-temperature jump point compensation method proposed for multipole magnetic encoder in this paper can effectively suppress the jump of angle value.

2. Model Establishment and Working Principle of Magnetic Encoder

The structure of the magnetic encoder studied in this paper is shown in Figure 1. It consists of single-pole magnetic steel, multipole magnetic steel, and a signal detection board. The magnetic steel of the single-pole and multipole is bonded to the ends of the motor axle, and the signal detection board is installed above them. A1301A Hall elements are mounted on the signal detection board.

In this study, the pole number of the multipole magnetic steel is 16, which means it generates 16 cycles of the magnetic field signal when it rotates through 360°. The Hall element receives the magnetic field signal and generates an induced voltage. The induced voltage generates the digital signal through the A/D converter module of the MCU. The single-pole and multipole angle values of the magnetic encoder are calculated after the digital signal is obtained, and the mapping relation between the angle values of the single-pole and multipole is judged. The angle values of the multipole magnetic encoder after subdivision are obtained according to the subdivision algorithm of angle values [21]. The working principle of the magnetic encoder is shown in Figure 2. We can see from Figure 2 that the angle value signal of the single-pole and multipole of the magnetic encoder is detected by the Hall element, and the subdivision of the multipole angle values needs to be based on the mapping relationship between single-pole and multipole angle values.

However, the magnetic sensitivity of the Hall element varies at different temperatures; the change of the magnetic sensitivity coefficient will result in the change of the single-pole angle value and the multipole angle value. However, the subdivision process of the multipole angle value is completed according to the correspondence between the single-pole angle value and the multipole angle value. The change of the correspondence value of the angle value will inevitably lead to a change in the mapping relationship between the multipole angle value and the single-pole angle value. As shown in Figure 3, due to the change of the mapping relationship between the single-pole and multipole angle values calculated by the Hall element, it leads to errors in the multipole angle value subdivision calculation. Eventually, it leads to a judgment error, as it causes the interval critical position for subdivision of the angle value of a multipole magnetic encoder to appear as an angle jump point.

To improve the stability of a multipole magnetic encoder working in different temperature environments, it is necessary to analyze its magnetic field signal and the temperature field characteristics. Moreover, an angle value error compensation strategy needs to be proposed for the

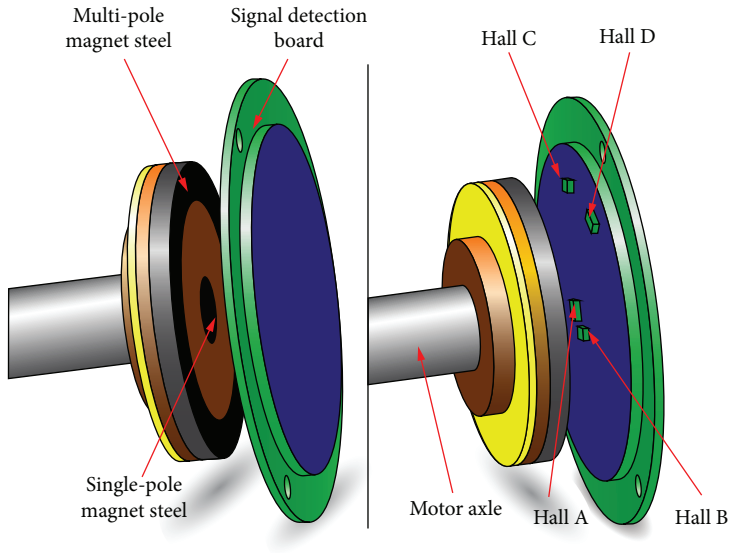

Figure 1: The structure of the magnetic encoder.

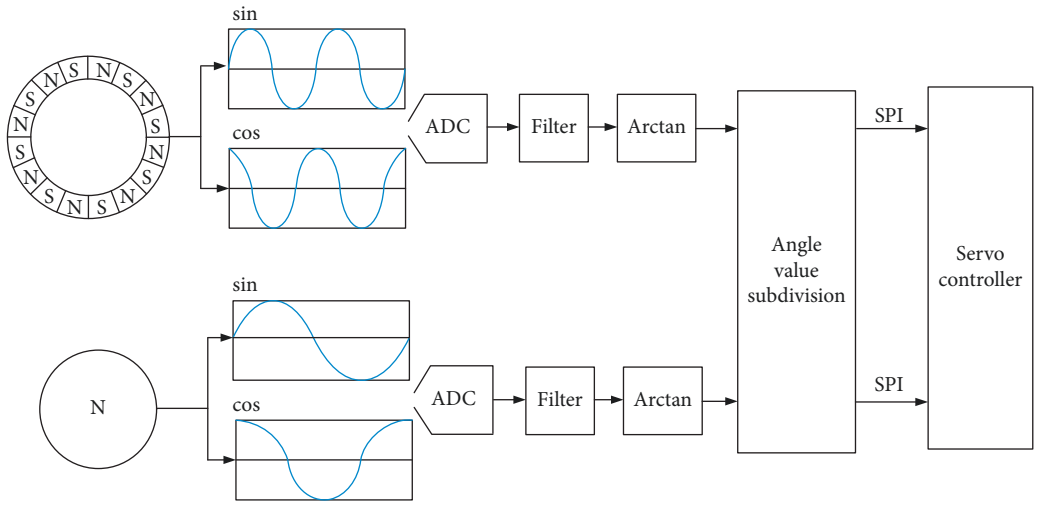

Figure 2: The working principle of the magnetic encoder.

angle value errors caused by the temperature field and the magnetic field change.

3. Simulation Analysis of the Magnetic Encoder

3.1. Temperature Field Caused by Eddy Current Loss. To consider the temperature effects of eddy current losses, we have given the solution domain model of a 3D transient magnetic field for the magnetic encoder, which is shown in Figure 4. The solution domain model of a 3D transient magnetic field includes multipole magnetic steel, single-pole magnetic steel, a signal detection board, and a Hall element. The multipole and single-pole magnetic steel are rotated at 300 rad/min in the process of solving the 3D transient electromagnetic field.

The mathematical model of the 3D transient magnetic field of the magnetic encoder is given

$$\begin{cases} \nabla \cdot \mu(\mathrm{T} - \nabla\psi) = -\nabla \cdot \mu \mathrm{H}_s, \\ \nabla \times \rho \nabla \times \mathrm{T} - \nabla\rho \nabla \cdot \mathrm{T} + \dfrac{\partial \mu(\mathrm{T} - \nabla\psi)}{\partial t} + \dfrac{\partial \mu \mathrm{H}_s}{\partial t} = 0, \end{cases} \tag{1}$$

where T is the electric vector potential, ψ is the scalar magnetic potential, μ is the permeability (in H/m), ρ is the resistivity (in $\Omega \cdot$ m), and t is the time (in s).

The magnetic field distribution in the 3D transient magnetic field of the magnetic encoder is shown in Figure 5. The magnetic density distribution of the Hall element is shown in Figure 6. It can be seen that the magnetic density is induced

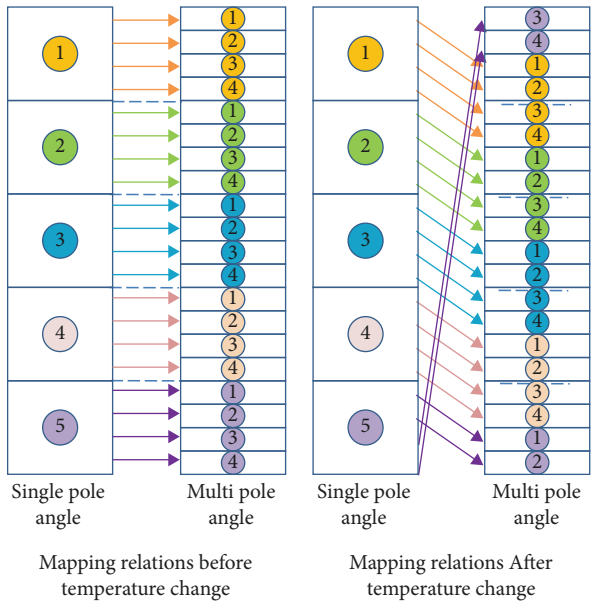

Figure 3: The magnetic sensitivity of the Hall element.

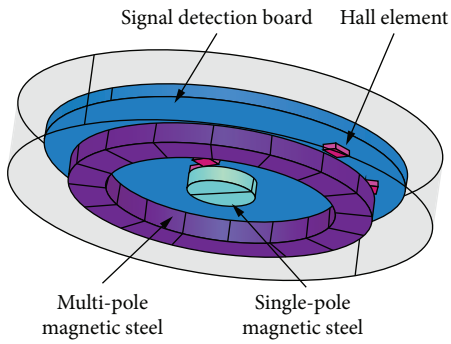

Figure 4: The solution domain model of a 3D transient magnetic field.

in the Hall element under the effect of the rotating magnetic field generated by the multipole and single-pole magnetic steel, and the maximum magnetic density of the Hall element is 0.33463 T.

To study the temperature field of the magnetic encoder in detail, we have given the solution domain model of the temperature field for the magnetic encoder, which is shown in Figure 7. The heat losses of the Hall element and signal detection board calculated by the 3D transient magnetic field were used as the heat sources in the temperature field analysis, and then the temperature distribution of the Hall element and the signal detection board can be accurately determined after solving the 3D temperature field equation. The 3D equation of temperature field is

$$\frac{\partial}{\partial x}\left(\lambda_x \frac{\partial T}{\partial x}\right) + \frac{\partial}{\partial y}\left(\lambda_y \frac{\partial T}{\partial y}\right) + \frac{\partial}{\partial z}\left(\lambda_z \frac{\partial T}{\partial z}\right) + q_v = \rho c \frac{\partial T}{\partial t}, \tag{2}$$

where λ_x, λ_y, and λ_z denote the thermal conductivity coefficient in the x, y, and z directions, respectively, and q_v denotes the heat density.

The ambient temperature is set as 25°C, and the natural heat dissipation boundary condition is adopted in the process of solving the 3D temperature field. The temperature distribution of the magnetic encoder is shown in Figure 8. It can be seen that the maximum temperature rise of the magnetic encoder is 0.1427 K. This indicates that the magnetic encoder will generate a temperature rise with the rotation of the magnetic steel. However, as the temperature rise is small, we can ignore the effect of eddy current loss on temperature.

3.2. Simulation of a Static Magnetic Encoder. We can see from the above analysis that the influence of the magnetic field generated by mechanical rotation on the temperature rise of the Hall element can be neglected. Now, the influence of temperature change on the Hall element output signal is analyzed when the magnetic encoder is stationary. The magnetic encoder and permanent magnet synchronous motor (PMSM) are coaxially installed. Then, the motor rotor position is fixed at normal and low temperatures. The measured output values corresponding to Hall A and Hall B, which are single-pole Hall elements, are shown in Figures 9 and 10.

We can see from Figures 9 and 10 that the output angle values of Hall A and Hall B are different at normal and low temperatures. The magnetic sensitivity coefficient of the Hall element changes with temperature changes, which leads to changes in the output voltages of Hall A and Hall B.

The output voltages of Hall A and Hall B at low temperature are derived as

$$\begin{cases} V_A = D \sin(k\pi) + \Delta T, \\ V_B = D \cos(k\pi) + \Delta T, \end{cases} \tag{3}$$

where V_A is the output voltage of Hall A; V_B is the output voltage of Hall B; $\triangle T$ is the temperature variation coefficient error; and D is the signal amplitude. The ADC module of the MCU used in this study is 12 bits, so the range of signal amplitude is 0–4095(2^12-1).

The output voltages of Hall A and Hall B at a normal temperature are derived as

$$\begin{cases} V_A = D \sin(k\pi), \\ V_B = D \cos(k\pi). \end{cases} \tag{4}$$

To calculate the angle value, divide the angle value into eight intervals based on the relationship between V_A and V_B as shown in Figure 11. When V_A and V_B are in the first interval, then $\theta = \tan^{-1}(V_B/V_A)$. When V_A and V_B are in the second interval, then $\theta = (\pi/2) - \tan^{-1}(V_A/V_B)$. When V_A and V_B are in the third interval, then $\theta = (\pi/2) + \tan^{-1}(-V_A/V_B)$. When V_A and V_B are in the fourth interval part, then $\theta = \pi - \tan^{-1}(V_B/-V_A)$. When V_A and V_B are in the fifth interval, then $\theta = 2\pi - \tan^{-1}(-V_B/V_A)$. When V_A and V_B are in the sixth interval, then $\theta = (3\pi/2) + \tan^{-1}(V_A$

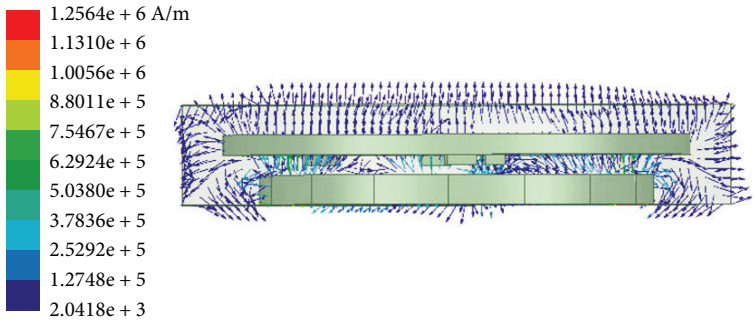

Figure 5: The magnetic field distribution in the 3D transient magnetic field.

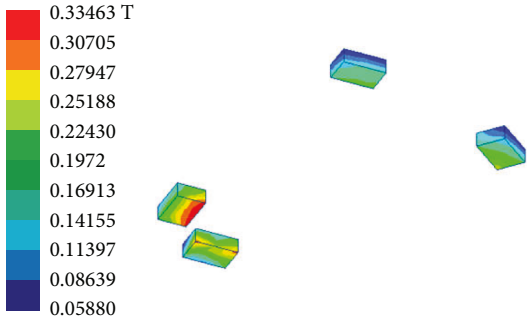

Figure 6: The magnetic density distribution of the Hall element.

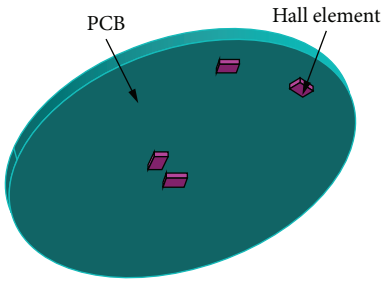

Figure 7: The solution domain model of temperature field.

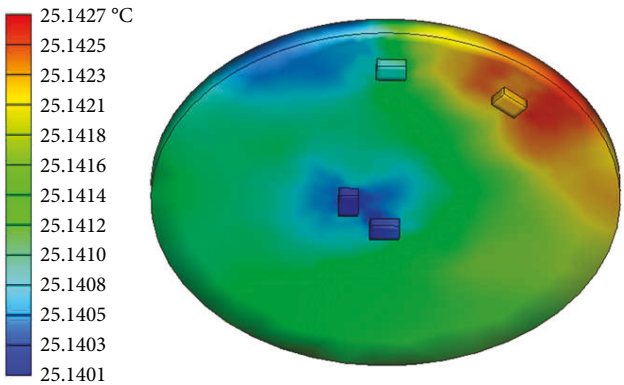

Figure 8: The temperature distribution of the magnetic encoder.

$/-V_B$). When V_A and V_B are in the seventh interval, then $\theta = (3\pi/2) - \tan^{-1}(V_A/V_B)$. When V_A and V_B are in the eighth interval, then $\theta = \pi + \tan^{-1}(V_B/V_A)$.

According to equations (3) and (4), the influence of signal amplitude D and temperature variation coefficient error $\triangle T$ on angle value accuracy is studied, when $D = 1024$ and $\triangle T = 50$, as shown in Figure 12(a); when $D = 512$ and $\triangle T = 50$, as shown in Figure 12(b); and when $D = 1024$ and $\triangle T = 200$, as shown in Figure 12(c). It can be seen from Figures 12(a) and 12(b) that the angle value deviation increases with a decrease in the amplitude of the angle value. Furthermore, it can be seen from Figures 12(a) and 12(c) that the deviation between the ideal angle value and actual angle value increases with an increase in the temperature variation coefficient error.

It can be seen from Figure 12 that the angle value deviation decreases with an increase in the angle amplitude of the magnetic encoder under the same temperature variation coefficient error. Furthermore, the angle value deviation increases with an increase in the temperature variation coefficient error when the signal amplitude is the same.

The above simulation analysis reveals that the greater the magnetic field of the encoder, the lower the influence of changes in the temperature field on the angle value. Furthermore, the deviation of angle value increases with an increase in the temperature field under the same magnetic field intensity. The temperature rise of the Hall element caused by the temperature field exists objectively. To improve the anti-interference ability of the magnetic encoder, it is necessary to improve the amplitude of the received signal of the magnetic encoder. Therefore, the strong sensitive Hall A1301KUA-T is used as the sensor chip and the strong magnetic material N-40UH is used as the permanent magnet for the magnetic encoder in this paper.

4. Jump Point Suppression Method for Multipole Angle Values at Low Temperature Based on Single-Pole Angle Value Fitting

4.1. Multiwindow Interval Prediction Angle Subdivision. The single-pole and multipole angle values of the magnetic encoder have synchronized acquisition at normal temperature. We can obtain the subdivided multipole angle values by using the multiwindow interval prediction angle subdivision method [21]. The working process of the angle value subdivision of the magnetic encoder is as follows. First, the upper window, current window, and lower window of the

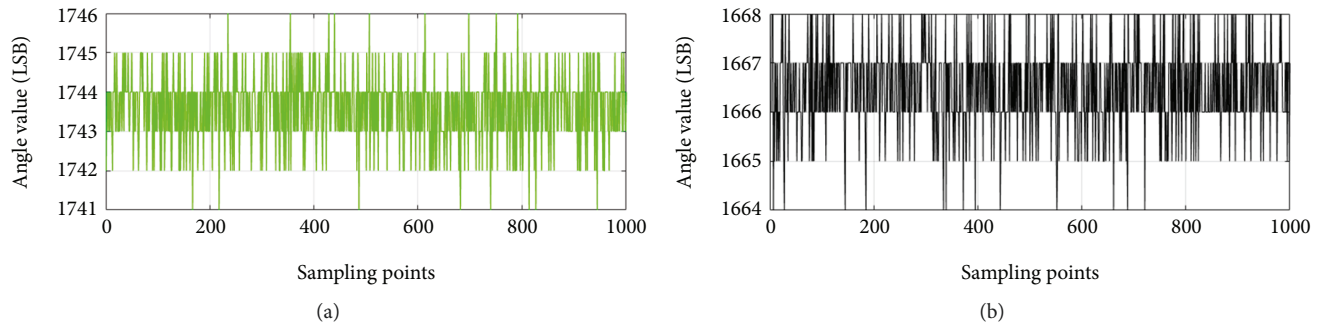

Figure 9: The output angle value of Hall A and Hall B at normal temperature. (a) The output angle value of Hall A. (b) The output angle value of Hall B.

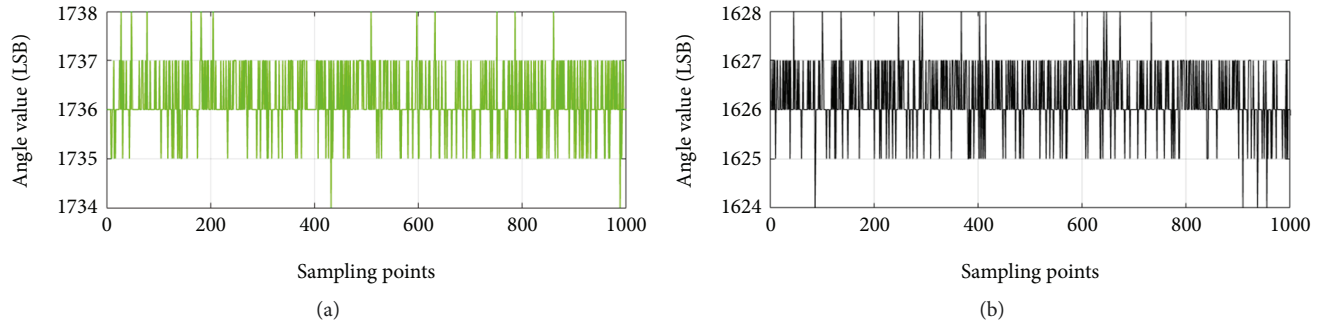

Figure 10: The output angle value of Hall A and Hall B at low temperature. (a) The output angle value of Hall A. (b) The output angle value of Hall B.

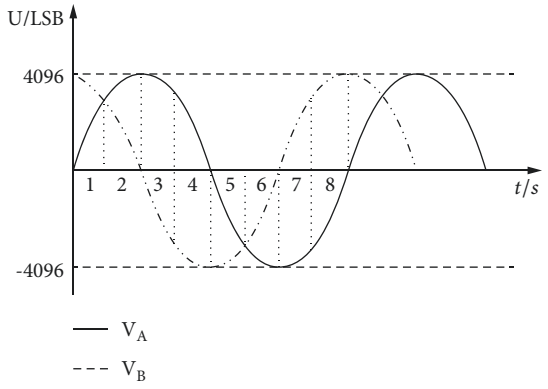

Figure 11: The interval segmentation of V_A and V_B.

multipole angle values can be constructed according to the obtained multipole angle value, which is

$$\begin{cases} N_1 = N + N_w, \\ N_2 = N, \\ N_3 = N - N_w, \end{cases} \tag{5}$$

where N is the angle value of the multipole; N_1 is the angle value of the upper window; N_2 is the angle value of the current window; N_3 is the angle value of the lower window; and N_w is the window amplitude.

Collect the multiple pole angle values through experiments, and the window value is set to 25000 (the range of multipole angle values is 0–65535 LSB). The upper window, lower window, and current window are shown in Figure 13 based on equation (5).

We can obtain the mapping table of the upper window angle value, the current window angle value, and the lower window angle value corresponding to the single-pole angle value. Then, the pole number of the current window angle value is judged logically according to the mapping table. Finally, the pole number of the current window angle value is obtained. The process of angle subdivision is shown in Figure 14.

The multipole angle values after subdivision through experiment are shown in Figure 15, and the differential values of the multipole angle values after subdivision are shown in Figure 16. We can see from Figure 16 that the multipole angle values after subdivision are smooth and no jump points exist.

In the same way, we use the mapping table in Figure 14 to subdivide the multipole angle values in a low-temperature environment. We can see from the three parts of the simulation analysis that the angle values of single-pole and multipole will change with changes in the temperature. The changes in the angle value $\triangle\theta$ will directly lead to dislocation of the table mapping relation when looking up the table, which is shown in Figure 17.

At this time, we still use the table shown in Figure 14 to subdivide the angle values of the multipole magnetic encoder,

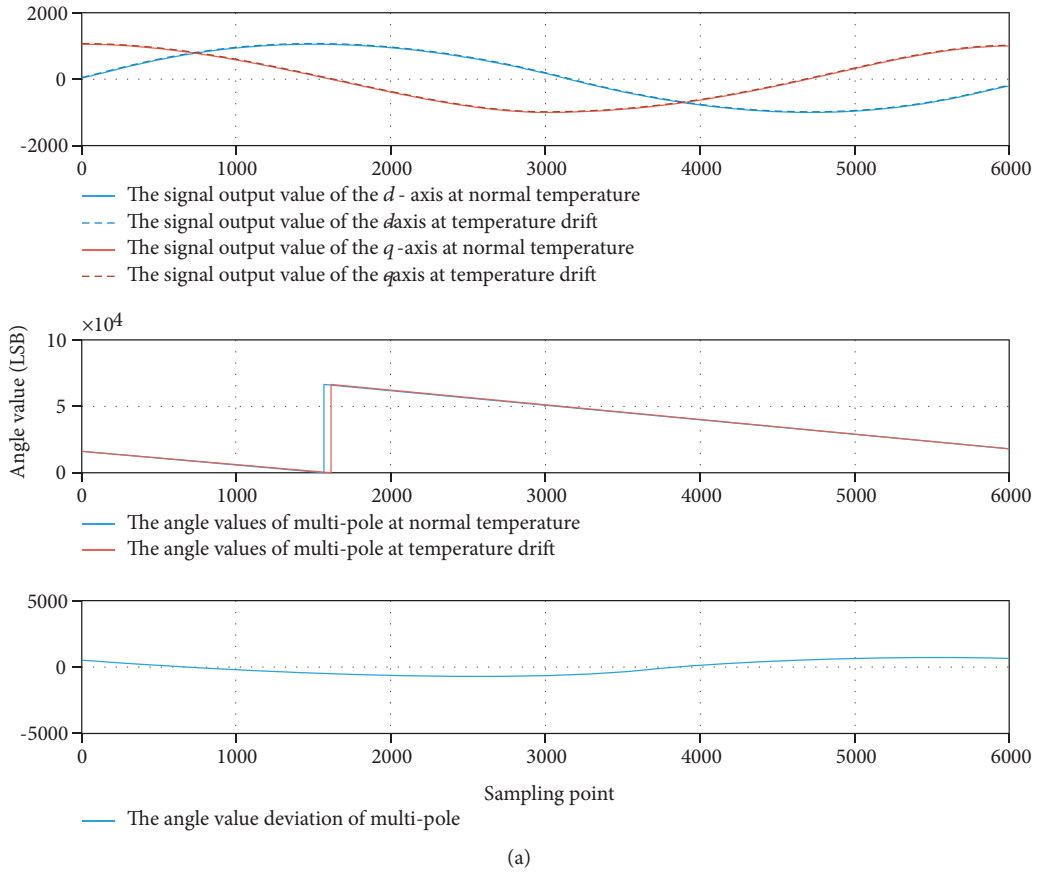

(a)

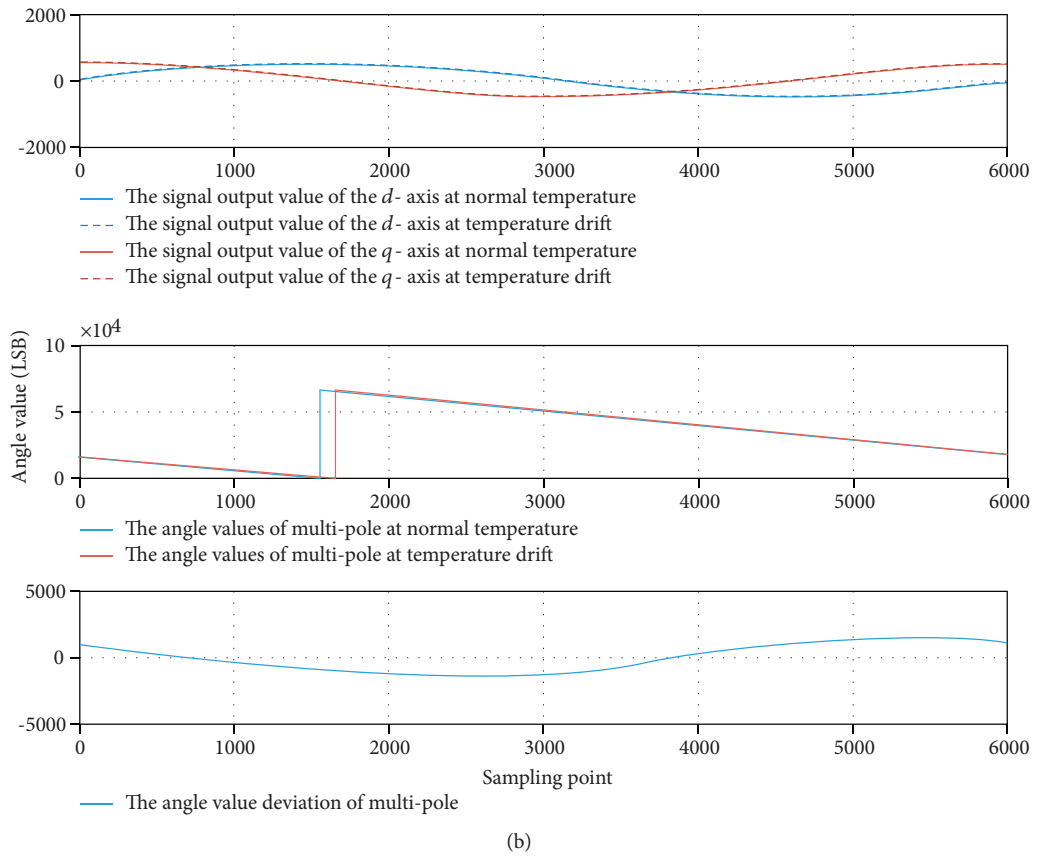

(b)

Figure 12: Continued.

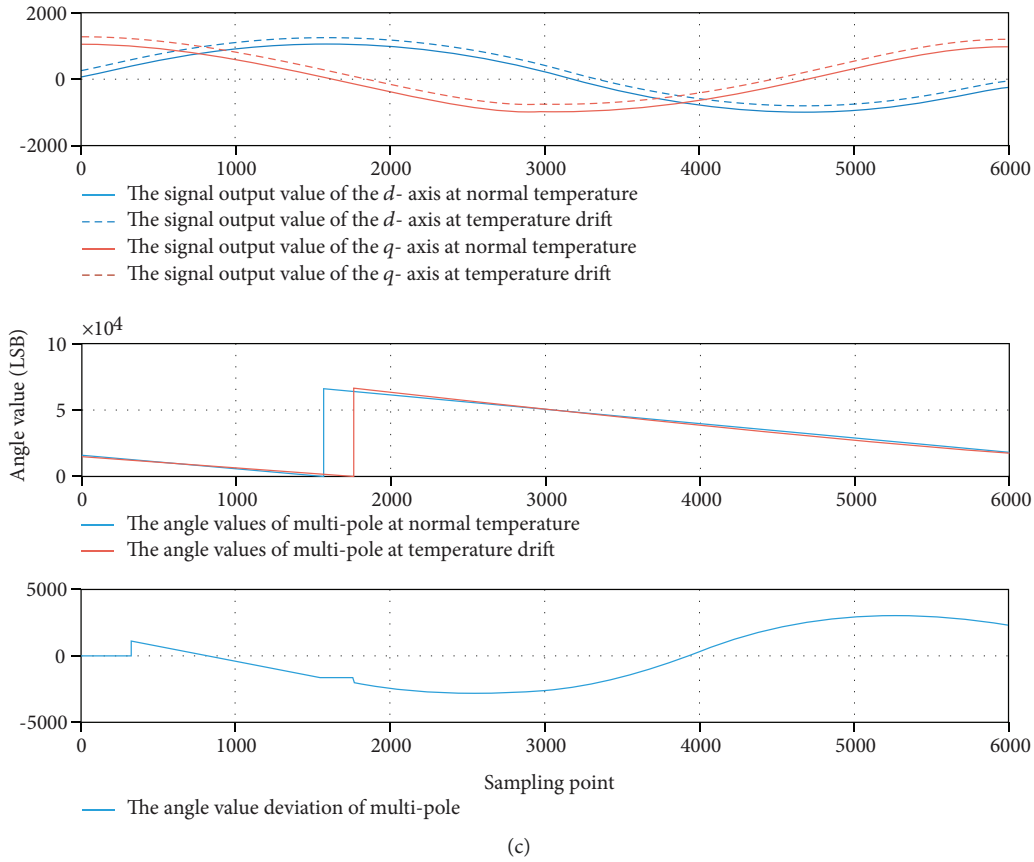

(c)

Figure 12: The influence of signal amplitude and temperature variation coefficient error on angle value accuracy. (a) When $D = 1024$ and $\triangle T = 50$. (b) When $D = 512$ and $\triangle T = 50$. (c) When $D = 1024$ and $\triangle T = 200$.

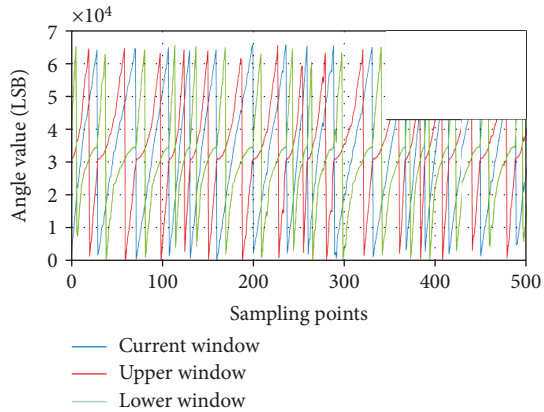

Figure 13: The window angle values of the multipole encoder.

and the angle value waveform of the subdivision is shown in Figure 18. The differential value of the angle value after subdivision is shown in Figure 19.

We can see from Figure 19 that the angle value is jumping at some positions and the jump value is fixed. According to the above analysis, this jump is mainly caused by the subdivision of the table using the angle value subdivision. It can be seen, based on the above analysis, that this jump is mainly caused by the mapping relationship error of the table when the angle value is subdivided.

To eliminate the jump points of multipole angle values after subdivision for the magnetic encoder at low temperatures, the suppression method of jump points for multipole angle values at low temperatures based on single-pole angle value fitting is proposed in this paper.

4.2. Jump Point Suppression Method for Multipole Angle Values. Simulation analysis of the angular value subdivision process at low temperature has been done; the angle value subdivision table is checked by using the single-pole angle value in a low-temperature environment, and the angle value of the multipole magnetic encoder after subdivision is obtained. The multipole angle value after subdivision is synchronized with the single-pole angle value, as shown in Figure 20.

Although we are aware of the harmful effects of temperature on the angle division process of the magnetic encoder, we do not know the specific position that is affected. We can see from Figure 21 that there are many jump points in the multipole angle value after the subdivision, but there are no jump points in the single-pole angle values. This is because the multipole angle value subdivision process needs the relationship between the single-pole angle and multipole angle, and changes in the mapping relationship will directly lead to incorrect angle values. However, the calculation process of the single-pole angle does not have this process, so there is no jump point in the single-pole angle value.

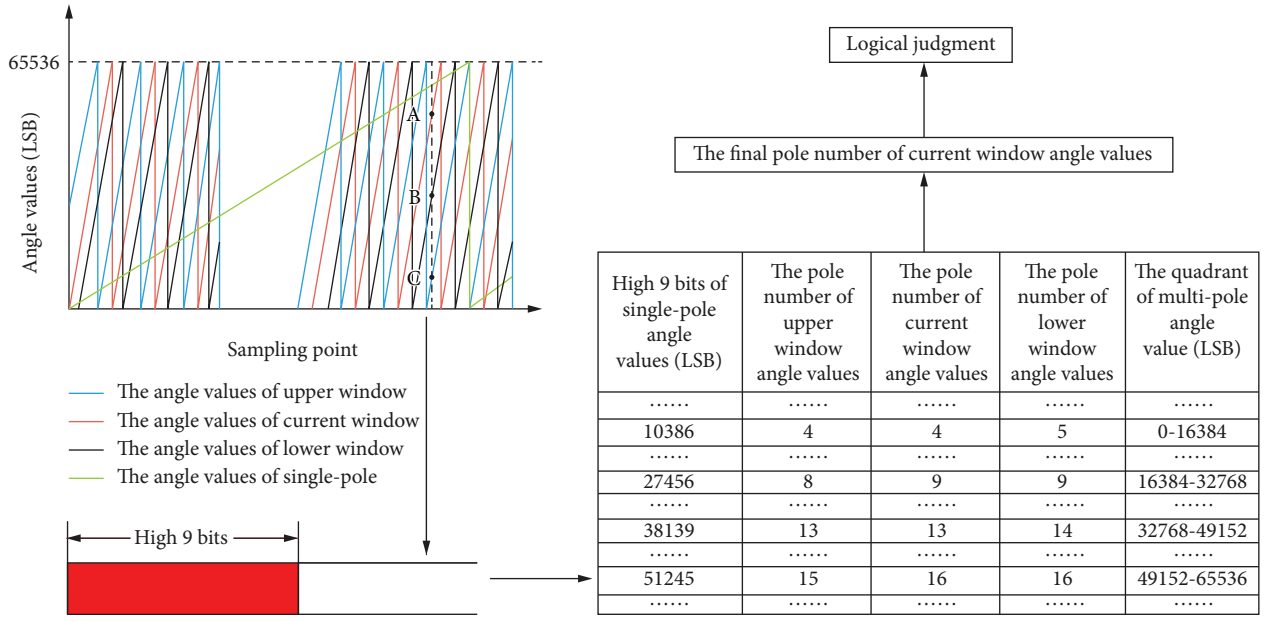

High 9 bits of single-pole angle values (LSB)	The pole number of upper window angle values	The pole number of current window angle values	The pole number of lower window angle values	The quadrant of multi-pole angle value (LSB)
.....	.....	.....	.....	.....
10386	4	4	5	0-16384
.....	.....	.....	.....	.....
27456	8	9	9	16384-32768
.....	.....	.....	.....	.....
38139	13	13	14	32768-49152
.....	.....	.....	.....	.....
51245	15	16	16	49152-65536
.....	.....	.....	.....	.....

Figure 14: The process of the angle subdivision.

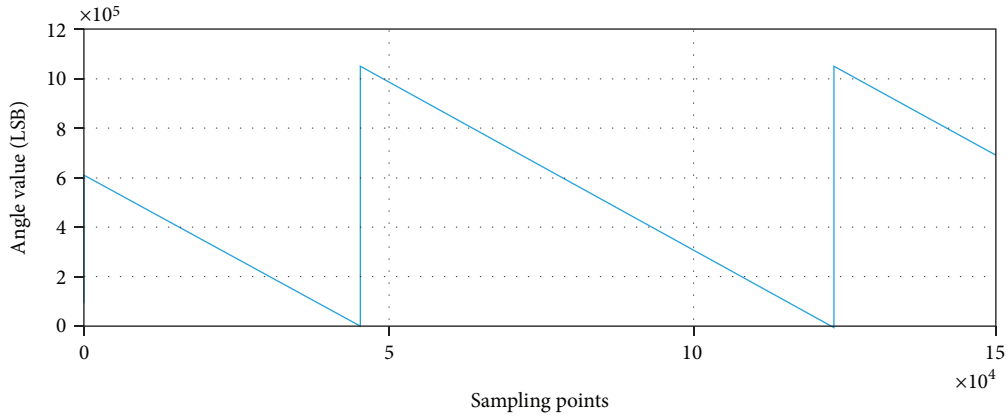

Figure 15: The subdivided angle values of multipole.

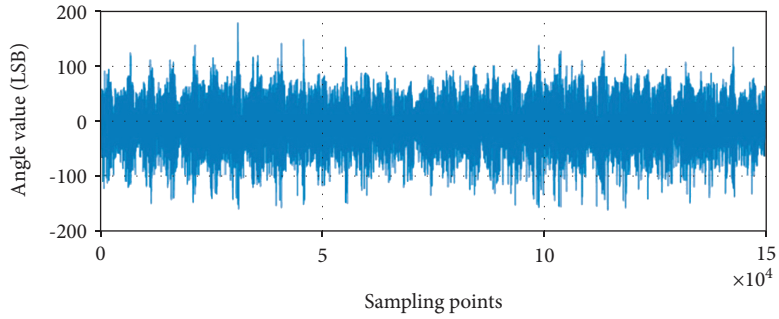

Figure 16: The differential value of multipole angle values after subdivision.

We can see from the above analysis that no single-pole angle value jump points are observed even with temperature changes. However, the resolution of the single-pole angle value is low, and the noise of the static angle value is large. In view of the above characteristics of the single-pole angle value, we use a method of fitting a single-pole angle value to a multipole angle value to determine the specific position of jump points for the multipole

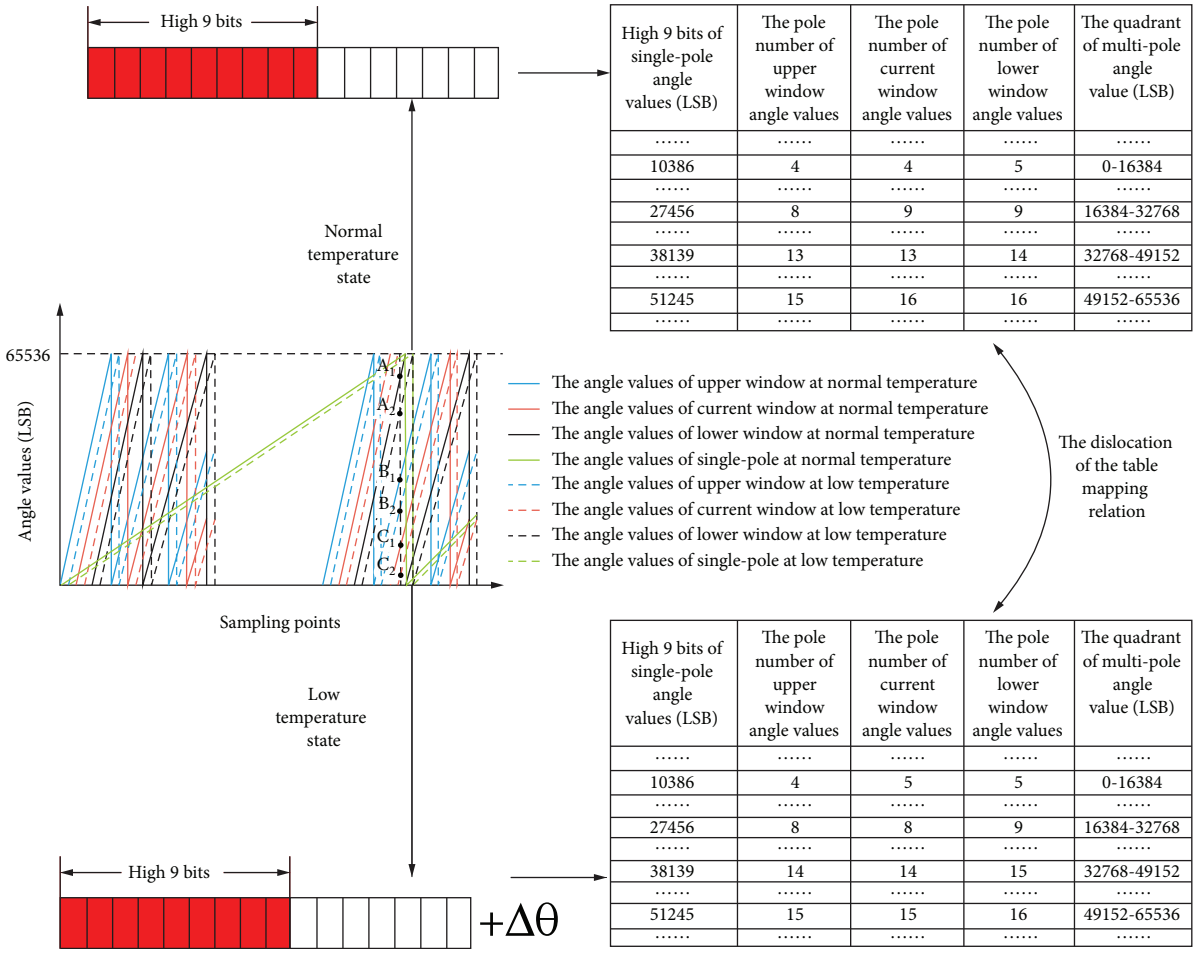

High 9 bits of single-pole angle values (LSB)	The pole number of upper window angle values	The pole number of current window angle values	The pole number of lower window angle values	The quadrant of multi-pole angle value (LSB)
……	……	……	……	……
10386	4	4	5	0-16384
……	……	……	……	……
27456	8	9	9	16384-32768
……	……	……	……	……
38139	13	13	14	32768-49152
……	……	……	……	……
51245	15	16	16	49152-65536
……	……	……	……	……

High 9 bits of single-pole angle values (LSB)	The pole number of upper window angle values	The pole number of current window angle values	The pole number of lower window angle values	The quadrant of multi-pole angle value (LSB)
……	……	……	……	……
10386	4	5	5	0-16384
……	……	……	……	……
27456	8	8	9	16384-32768
……	……	……	……	……
38139	14	14	15	32768-49152
……	……	……	……	……
51245	15	15	16	49152-65536
……	……	……	……	……

Figure 17: The table mapping relation at low temperature.

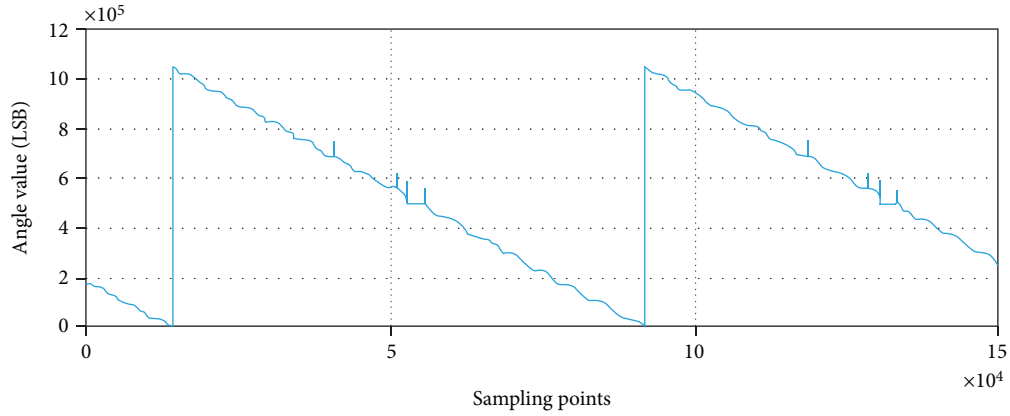

Figure 18: The subdivided angle values of multipole at low temperature.

angle values. The compensation value of the angle value jump error is determined by

$$\begin{cases} N_c = f(\theta_1, \theta_2, k_1, k_2, k_3), \\ N_d = f\left(\theta_1', \theta_2', k_1, k_2, k_3\right), \\ \Delta N = N_c - N_d, \end{cases} \tag{6}$$

where N_c is multipole angle values after subdivision at normal temperature; θ_1 is multipole angle values at normal temperature; θ_2 is single-pole angle values at normal temperature; N_d is multipole angle value after subdivision at low temperature; θ_1' is multipole angle values at low temperature; θ_2' is single-pole angle values at low temperature; k_1 is the pole number of the upper window; k_2 is the pole number of the current window; k_3 is the pole number

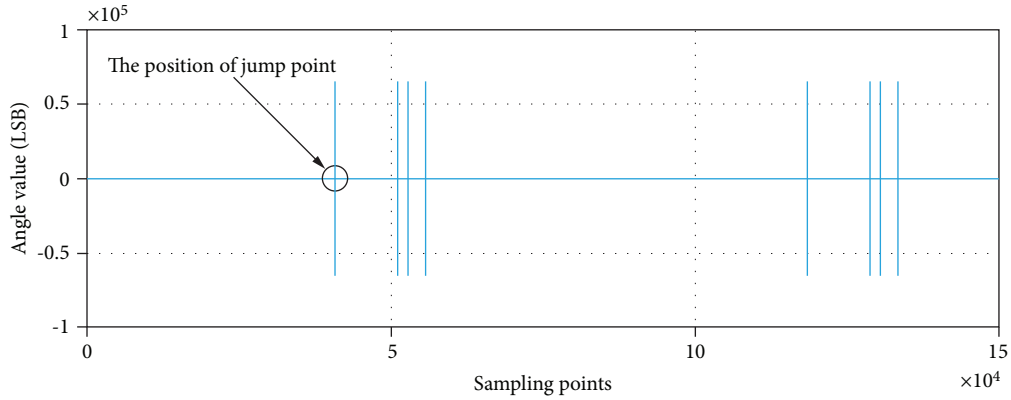

Figure 19: The differential value of multipole angle value after subdivision at low temperature.

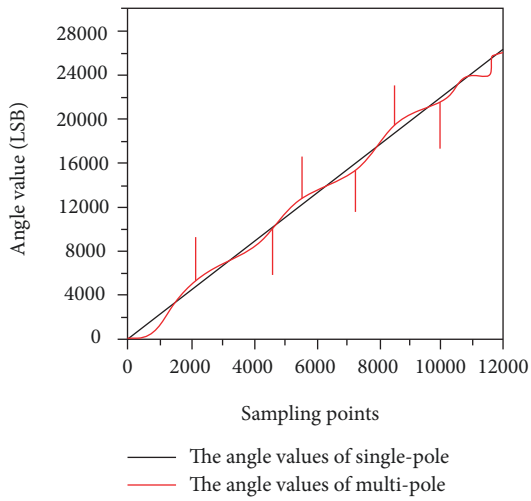

Figure 20: The angle values of single-pole and multipole at low temperature.

of the lower window; and ΔN is the deviation of angle value at normal and low temperatures.

By comparing the single-pole and multipole angle values at normal temperature, we can obtain the angle deviation between them, which we can use to generate the error compensation table of the angle values. To eliminate noise signals and ensure the precision of the compensation table, the oversampling linear interpolation tabulation method was utilized [22] according to the principle of oversampling. First, the sampling points were divided into 512 intervals based on the single-pole angle value (high 9 bits of single-pole angle value), and a coordinate system was established that made the interval number the abscissa, and the angle deviation between the single-pole angle value and multipole angle value the ordinate. Each six intervals as an oversampling data, if we want to obtain the 324^{th} interpolation, we can use the 318^{th} to 324^{th} intervals to calculate the mean error y_1 and the 324^{th} to 330^{th} intervals to calculate the mean error y_2. Finally, we can obtain the linear interpolation of the 324^{th} interval value based on y_1 and y_2. The principle of the oversampling linear interpolation method is shown in Figure 21. In this way, the interpolation of each point can be obtained, and the process of single-pole angle value error fitting tabulation can be completed.

The single-pole angle values can be fitted to the multipole angle values according to the above method. However, the resolution of the single-pole angle values is lower than that of the multipole angle values, so the static noise error of the single-pole angle values is larger than that of the multipole angle values. We can see from Figures 22(a) and 22(b) that the static error noise range of the single-pole angle values is [−400, 400] and the static error noise range of the multipole angle values is [−150, 150]. Due to the influence of the power noise and the external magnetic field when the magnetic encoder is working, the angle error range is set as $\Delta N \in [-2000, 2000]$. The range of the angle deviation of the multipole angle values and single-pole angle values after lookup in the mapping table is $\Delta J \in [-6000, 6000]$, which is shown in Figure 22(c). If $\Delta N/\Delta J < 33\%$, we can assume that the point is not a jump point. If $\Delta N/\Delta J > 33\%$, we can assume that this point is a jump point.

Because the pole number of the multipole magnetic steel is 16, we can see from equation (6) that the jump point is fixed at 65536/16 = 4096 (the range of multipole angle values of the integer cycle after subdivision is 0–65535). When $2000 < \Delta J < 6000$, we can eliminate the jump point by using

$$N_4 = N + 4096, \tag{7}$$

where N_4 is the multipole angle value after the jump points are eliminated, and $N_4 \in (0, 65536)$.

When $-6000 < \Delta J < -2000$, we can eliminate the jump point by using

$$N_4 = N - 4096. \tag{8}$$

5. Experiment

The magnetic encoder proposed in this paper was experimentally studied using Russells' QW501 model thermostat. Figure 23(a) shows the thermostat used in this paper which realizes the temperature change. Figure 23(b) shows the

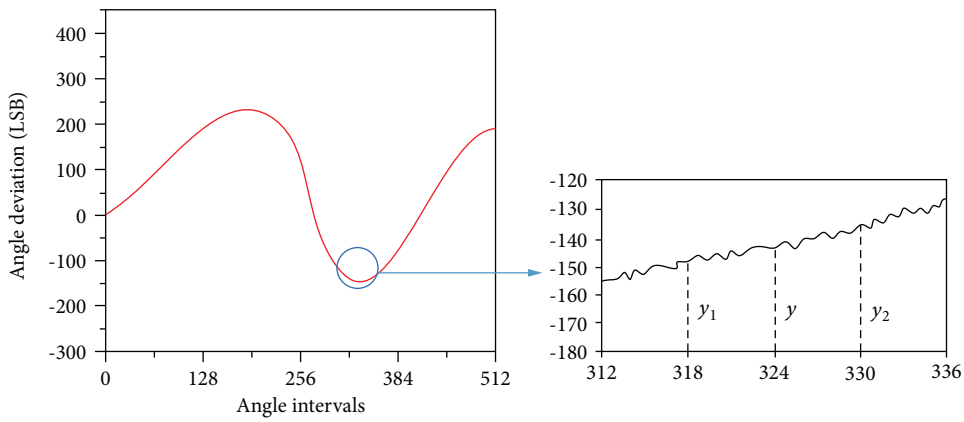

Figure 21: Principle of oversampling linear interpolation.

magnetic encoder proposed in this paper. The Micro Controller Unit (MCU) uses the Renesas' Rx62TADDFM 32-bit floating-point MCU and uses Serial Peripheral Interface (SPI) to communicate with the data acquisition card. The multipole angle signal passes through Texas Instruments' INA826 digital signal amplifier to realize the signal amplified. Utilize Texas Instruments' AMS117-5 as a power conversion chip to provide 5 V power to the system. Utilize Allegro's Hall A1301A as a sampling chip for single-pole and multipole magnetic signals. Figure 23(c) shows the magnetic steel of the magnetic encoder. The single-pole magnetic steel is made of N-40UH material, and the multipole magnetic steel which 16 poles is made of N-40UH material too. Figures 23(d) and 23(e) show the application of the magnetic encoder proposed in this paper with a 1 kW power permanent magnet synchronous motor (rated speed 3000 r/min, rated torque 3 Nm) which is driven by sensorless control method [8] to achieve a constant speed.

Experiments were conducted to prove the feasibility of this method; the experimental schematic diagrams are shown in Figure 24. Power was supplied to the motor and magnetic encoder through the power supply outside the thermostat. The servo controller uses a sensorless driving method to achieve constant rotation with a permanent magnet synchronous motor. The angle value is transmitted to the data acquisition card by SPI each 300 μs. The data acquisition card uses Renesas' RX62N MCU. When the data acquisition card collects the angle value, the data is transmitted to the computer through the USB, and the data acquisition process is controlled by computer interface.

Adjust the temperature in the thermostat, and keep each temperature point for an hour. Permanent magnet synchronous motor rotates at a constant speed of 25°/s with sensorless control method. Collect the angle value of the magnetic encoder, then judge whether there is a jump point in the angle value. The temperature command in the thermostat is shown in Figure 25.

At each temperature point, the sensorless drive motor method is used to drive the motor in forward and reverse rotation. The forward and reverse rotation angles are sampled 5 times, and the experimental results without the method proposed in this paper are shown in Table 1.

Under the normal temperature (25°C), the angle value with motor speed 25°/s is shown in Figure 26; Figure 26(a) is the forward rotation and Figure 26(b) is the reverse rotation.

Under the temperature -10°C (cool down), the angle value with motor speed 25°/s is shown in Figure 27; Figure 27(a) is the forward rotation and Figure 27(b) is the reverse rotation.

Under the temperature -20°C (cool down), the angle value with motor speed 25°/s is shown in Figure 28; Figure 28(a) is the forward rotation and Figure 28(b) is the reverse rotation.

Under the temperature -40°C (cool down), the angle value with motor speed 25°/s is shown in Figure 29; Figure 29(a) is the forward rotation and Figure 29(b) is the reverse rotation.

Under the temperature -20°C (warming up), the angle value with motor speed 25°/s is shown in Figure 30; Figure 30(a) is the forward rotation and Figure 30(b) is the reverse rotation.

Under the temperature -10°C (warming up), the angle value with motor speed 25°/s is shown in Figure 31; Figure 31(a) is the forward rotation and Figure 31(b) is the reverse rotation.

Under the temperature 25°C (warming up), the angle value with motor speed 25°/s is shown in Figure 32; Figure 32(a) is the forward rotation and Figure 32(b) is the reverse rotation.

We can see from Figures 26–32 that at normal temperature (25°C), there is no angle value jump point because the subdivision processing table for multipole angle values is established at normal temperature (25°C), and the angle value jump point appears during the cooling process because the table mapping relationship changes, resulting in an error in the angle value subdivision process. The jump point is characterized by a front-to-back angle difference, which is 4096 (65536/16) LSB. A full cycle angle resolution is 65536 LSB, and angle jump point value is 65536 divided by the magnetic pole number 16. In some experiments, no jump points occur at low temperature because the data acquisition process was intermittent (300 μs each time).

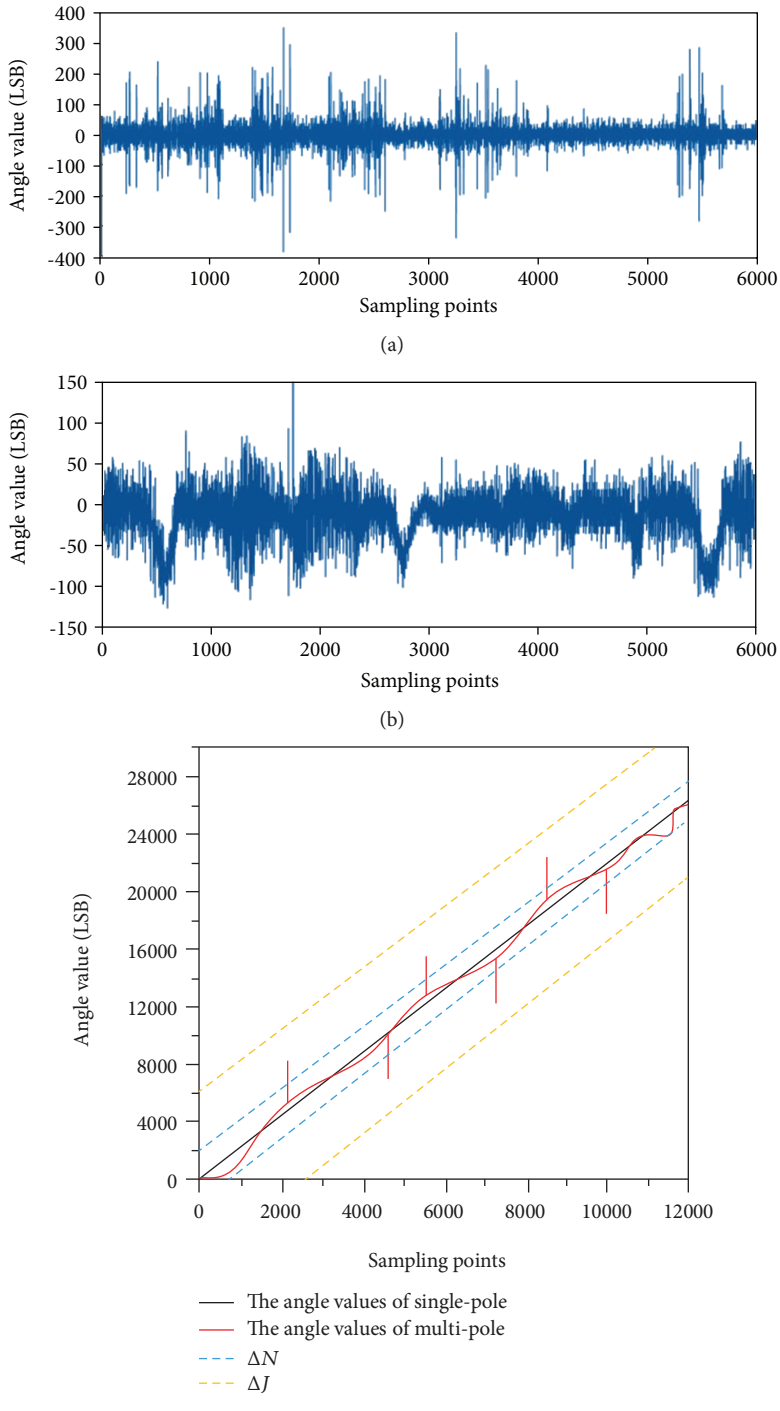

Figure 22: The principle of position judgment for jump points. (a) The noise signals of single-pole angle value. (b) The noise signals of multipole angle value. (c) The jump range of multipole angle values.

To demonstrate the effectiveness of method proposed in this paper, output angle value is obtained with the method proposed. As shown in Table 2, the experimental results show that no angle jump points occurred in all five experiments.

Figure 33 shows the subdivided angle values of the multipole magnetic encoder at −40°C with and without the method proposed in this paper. We can see from Figure 33(b) that the jump points were effectively eliminated, which proves the feasibility of the proposed method.

6. Conclusions

To eliminate the jump points of multipole angle values after subdivision at a low temperature, the magnetic field and

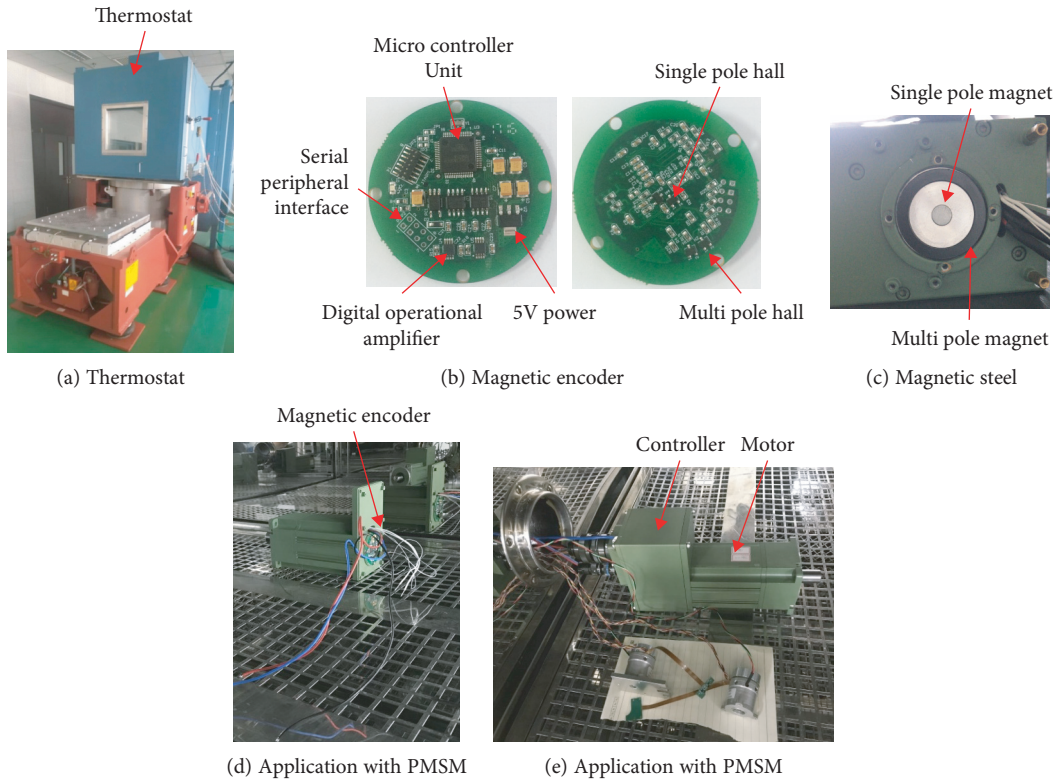

Figure 23: Hardware for magnetic encoder experiment.

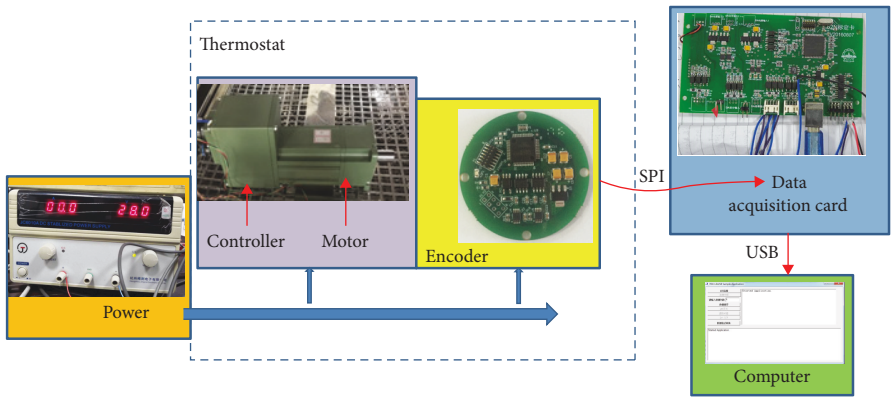

Figure 24: The experimental schematic diagram.

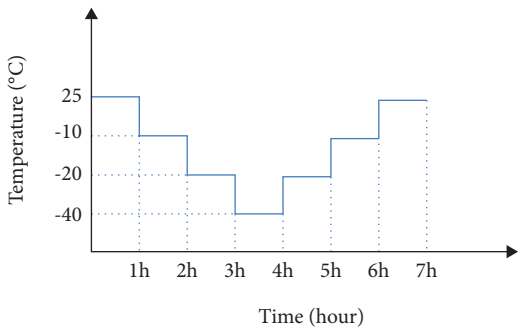

Figure 25: Temperature command.

Table 1: Without the method proposed in this paper.

Temperature point	Jump points occur with forward rotation	Jump points occur with reverse rotation	Rotor speed
25°C	0	0	25°/s
-10°C (cool down)	2	3	25°/s
-20°C (cool down)	4	4	25°/s
-40°C (cool down)	5	5	25°/s
-20°C (warming up)	3	4	25°/s
-10°C (warming up)	2	2	25°/s
25°C (warming up)	0	0	25°/s

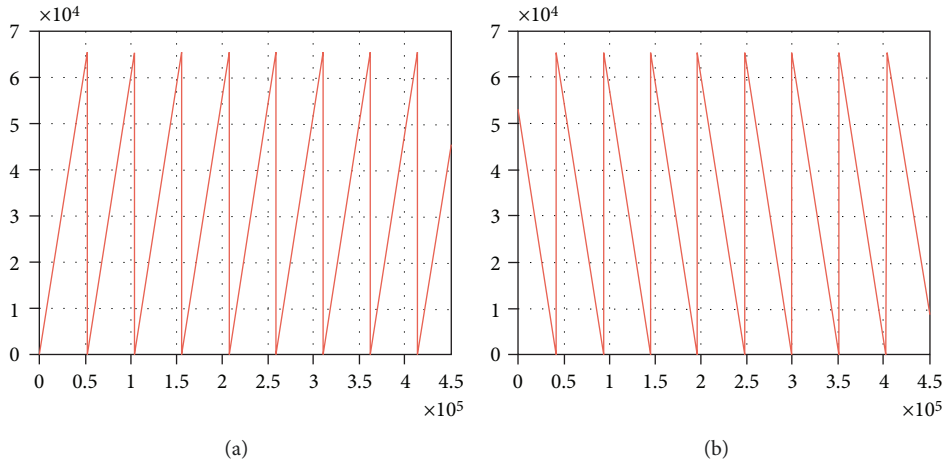

Figure 26: The output angle value (25°C).

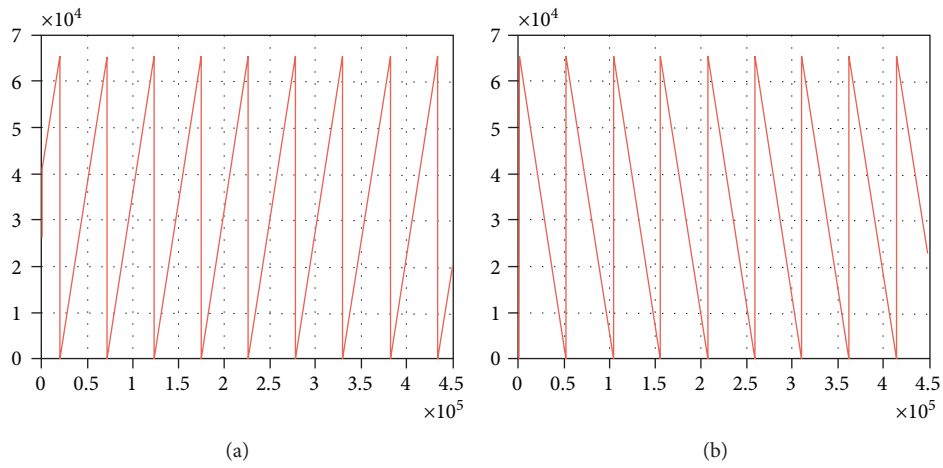

Figure 27: The output angle value (-10°C cool down).

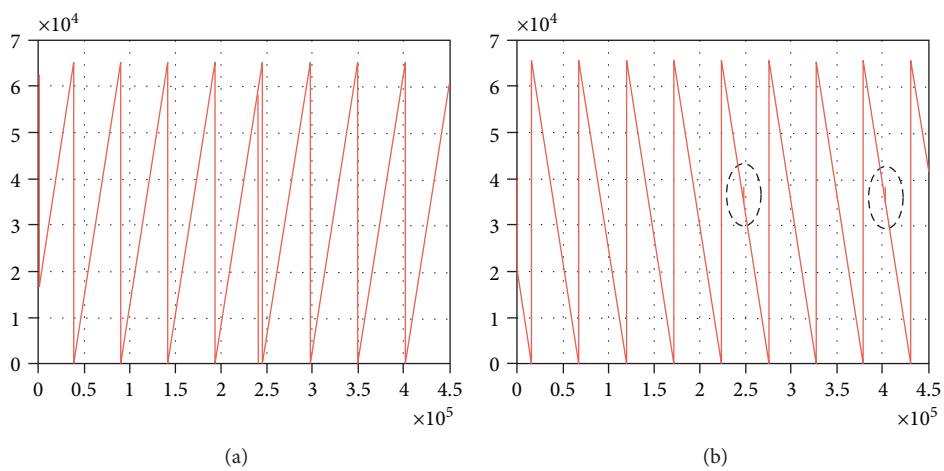

Figure 28: The output angle value (-20°C cool down).

temperature field characteristics of a multipole magnetic encoder were analyzed. The magnetic field loss generated by the magnetic encoder was used as the heat source of the temperature field analysis, and the effects of changes in magnetic field strength and temperature field on the precision of angle values were studied. To reduce the effect of changes in

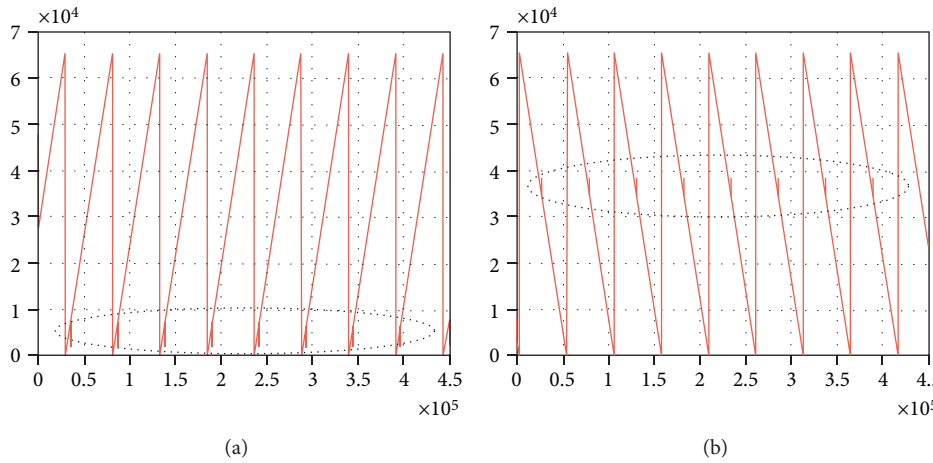

Figure 29: The output angle value (-40°C cool down).

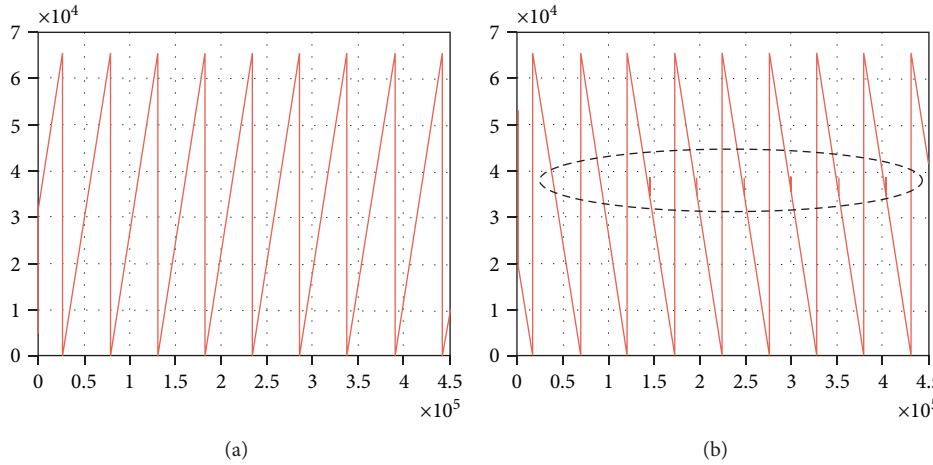

Figure 30: The output angle value (-20°C warming up).

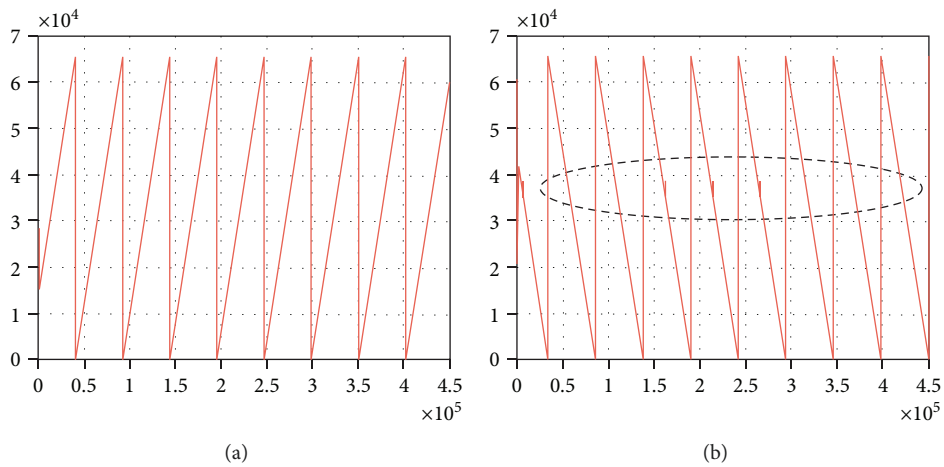

Figure 31: The output angle value (-10°C warming up).

the temperature field on the accuracy of the angle value signals, the amplitude of the angle value signals was improved by using a strong sensitive Hall element and strong magnetic field steel material. To eliminate the jump points of multipole angle values caused by changes in the temperature field, a suppression method based on single-pole angle value fitting

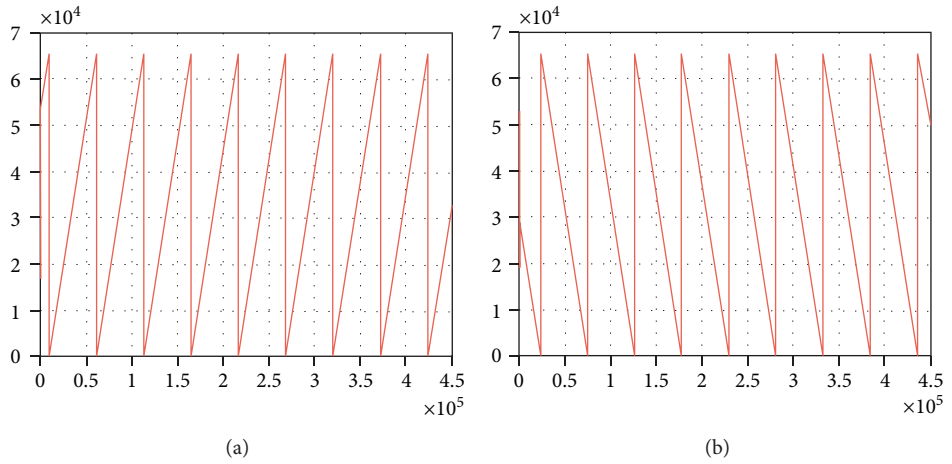

Figure 32: The output angle value (25°C warming up).

Table 2: With the method proposed in this paper.

Temperature point	Jump points occur with forward rotation	Jump points occur with reverse rotation	Rotor speed
25°C	0	0	25°/s
-10°C (cool down)	0	0	25°/s
-20°C (cool down)	0	0	25°/s
-40°C (cool down)	0	0	25°/s
-20°C (warming up)	0	0	25°/s
-10°C (warming up)	0	0	25°/s
25°C (warming up)	0	0	25°/s

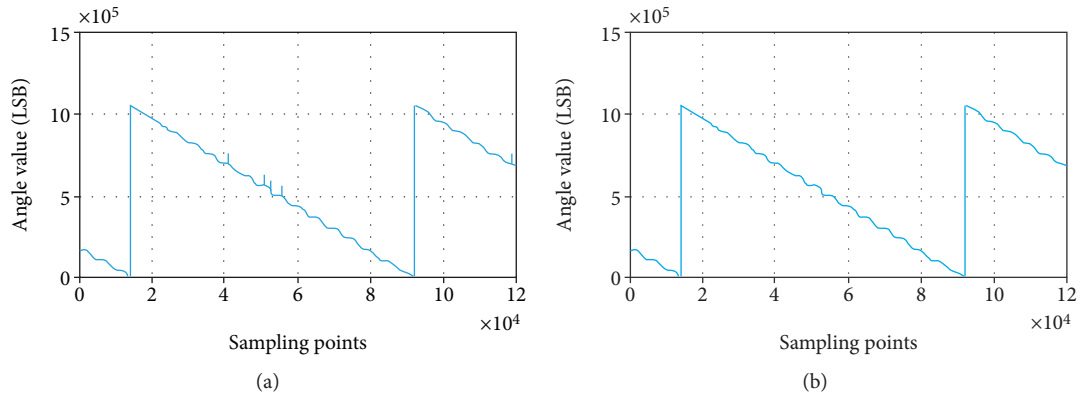

Figure 33: The subdivided angle values of multipole encoder at -40°C. (a) Before using the method proposed in this paper. (b) After using the method proposed in this paper.

was proposed. The errors between the single-pole and multipole angle values were tabulated by the oversampling linear interpolation method, and the precision of fitting single-pole to multipole angle values was effectively improved. The error of the angle value caused by the changes in the temperature field was studied and analyzed, and the relationship between the jump point angle values and the pole number of the multipole magnetic encoder was obtained. Furthermore, the jump points were compensated for by the jump range of the multipole angle values. Finally, the angle accuracy of the multipole magnetic encoder in a thermostat was experimentally verified. The experimental results reveal that the low-temperature jump point compensation method proposed for the multipole magnetic encoder in this study can effectively suppress the jump of angle values.

Data Availability

The original angle value data used to support the findings of this study have been deposited in the original angle value of magnetic encoder repository.

Conflicts of Interest

The authors confirm that this article content has no conflict of interest.

Acknowledgments

The authors wish to acknowledge the support from the China Postdoctoral Science Foundation (2016M600256), Postdoctoral Foundation in Heilongjiang Province (LBH-Z16092), Harbin Science and Technology Innovation Talent Research Special Fund Project (2017RAQXJ076), Heilongjiang Youth Innovation Talent Project (UNPYSCT-2018211), National Natural Science Foundation of China (51807043), China Postdoctoral Science Foundation (2018T110269, 2018M630336), and Fundamental Research Foundation for Universities of Heilongjiang Province (LGYC2018JC024).

Supplementary Materials

Supplementary 1. The original (The data at low temperature.txt) data used to support the findings of this study are included within the supplementary information file. The second column of the data is the single-pole angle value of the magnetic encoder. The fourth column of the data is the angle value of the photoelectric encoder, and the third column of the data is the multipole angle value of the magnetic encoder.

Supplementary 2. The original (The data at normal temperature.txt) data used to support the findings of this study are included within the supplementary information file. The first column of the data is the single-pole angle value of the magnetic encoder. The second column of the data is the angle value of the photoelectric encoder, and the fourth column of the data is the multipole angle value of the magnetic encoder.

References

[1] W. Gao, S. W. Kim, H. Bosse et al., "Measurement technologies for precision positioning," *CIRP Annals*, vol. 64, no. 2, pp. 773–796, 2015.

[2] A. '. A. M. Faudzi, K. Osman, M. F.'a. Rahmat, K. Suzumori, N.'m. D. Mustafa, and M. A. Azman, "Real-time position control of intelligent pneumatic actuator (IPA) system using optical encoder and pressure sensor," *Sensor Review*, vol. 33, no. 4, pp. 341–351, 2013.

[3] K. Nakano, T. Takahashi, and S. Kawahito, "A CMOS rotary encoder using magnetic sensor arrays," *IEEE Sensors Journal*, vol. 5, no. 5, pp. 889–894, 2005.

[4] S. Wang, J. Jin, T. C. Li, and G. Y. Liu, "High-accuracy magnetic rotary encoder," in *System Simulation and Scientific Computing*, T. Xiao, L. Zhang, and S. Ma, Eds., vol. 326 of Communications in Computer and Information Science, , pp. 74–82, Springer, 2012.

[5] Y. F. Zeng and F. F. Jiang, "Error compensation for single pair-pole encoder based on ellipse hypothesis," *Advanced Materials Research*, vol. 591-593, pp. 1231–1235, 2012.

[6] F. Jiang, D. Z. Lou, and H. Zhang, "Design of a GMR-based magnetic encoder using TLE5012B," in *2017 20th International Conference on Electrical Machines and Systems (ICEMS)*, pp. 1–4, Sydney, NSW, Australia, 2017.

[7] X. Wang, H. Wang, H. Xie, D. Lou, and K. Yang, "Design of magnetic encoder based on reconstructing and mapping looking-up table," in *Electrical Machines and Systems (ICEMS), 2016 19th International Conference*, pp. 1–4, Chiba, Japan, 2016.

[8] L. Wang, Y. Zhang, S. Hao, B. Song, M. Hao, and Z. Tang, "Study on high precision magnetic encoder based on PMSM sensorless control," *Sensor Review*, vol. 36, no. 3, pp. 267–276, 2016.

[9] S. M. Xiong, Y. Wang, X. Zhang, and D. Bogy, "A magnetic rotary encoder for patterned media lithography," in *2014 Conference on Information Storage and Processing Systems*, p. 4, Santa Clara, California, USA, 2014.

[10] Q. Wang, B. Zhang, Y. Tian, and M. M. Sun, "An absolute magnetic rotary encoder based on Kalman filter," in *The Twenty-fifth International Ocean and Polar Engineering Conference*, pp. 889–897, Kona, HI, USA, 2015.

[11] S.-T. Wu, J.-Y. Chen, and S.-H. Wu, "A rotary encoder with an eccentrically mounted ring magnet," *IEEE Transactions on Instrumentation and Measurement*, vol. 63, no. 8, pp. 1907–1915, 2014.

[12] T. Zou, F. L. Ni, and F. R. Li, "A new absolute magnetic encoder with big hallow," *Chinese Journal of Scientific Instrument*, vol. 7, pp. 1532–1538, 2016.

[13] H. T. Le, H. V. Hoang, and J. W. Jeon, "Efficient method for correction and interpolation signal of magnetic encoders," in *2008 6th IEEE International Conference on Industrial Informatics*, pp. 1383–1388, Daejeon, South Korea, 2008.

[14] A. N. Montanari and E. de Souza Oliveira, "A novel analog multisensor design based on fuzzy logic: a magnetic encoder application," *IEEE Sensors Journal*, vol. 17, no. 21, pp. 7096–7104, 2017.

[15] J. Lara, J. Xu, and A. Chandra, "A novel algorithm based on polynomial approximations for an efficient error compensation of magnetic analog encoders in PMSMs for EVs," *IEEE Transactions on Industrial Electronics*, vol. 63, no. 6, pp. 3377–3388, 2016.

[16] Y. L. Song, G. S. Chu, T. X. Ma, and R. M. Song, "Encoder subdivision method based on the software frequency doubling," *Chinese Journal of Scientific Instrument*, vol. 6, pp. 142–146, 2014.

[17] S. H. Hao and L. Yong, "Study on a novel absolute magnetic encoder," in *2008 IEEE International Conference on Robotics and Biomimetics*, pp. 1773–1776, Bangkok, Thailand, 2008.

[18] Y. Q. Feng and Q. H. Wan, "Interpolation error calibration method of small photoelectric encoder," *Chinese Journal of Scientific Instrument*, vol. 6, pp. 1374–1379, 2008.

[19] L. Wang, S.-H. Hao, B.-Y. Song, and M.-H. Hao, "Study on the temperature drift adaptive compensation algorithm of a magneto-electric encoder based on a simple neuron," *Journal of Power Electronics*, vol. 14, no. 6, pp. 1254–1262, 2014.

[20] Z. Zhang, F. Ni, Y. Dong, C. Guo, M. Jin, and H. Liu, "A novel absolute magnetic rotary sensor," *IEEE Transactions on Industrial Electronics*, vol. 62, no. 7, pp. 4408–4419, 2015.

[21] T. Feng, S. Hao, M. Hao, and J. Wang, "Development of a combined magnetic encoder," *Sensor Review*, vol. 36, no. 4, pp. 386–396, 2016.

[22] L. Wang, P. Li, Y. Qiao, S. Hao, and M. Hao, "Study on high precision magnetic encoder based on the arctangent cross-intervals tabulation method," *Australian Journal of Electrical and Electronics Engineering*, vol. 13, no. 3, pp. 167–173, 2017.